Solid State Communications 341 (2022) 114575

Contents lists available at ScienceDirect

Solid State Communications

journal homepage: www.elsevier.com/locate/ssc

Electrical properties and conduction mechanisms of heavily iron implanted silicon diodes

J.O. Bodunrin, S.J. Moloi *

Department of Physics, College of Science, Engineering and Technology, University of South Africa, Private Bag X6, Florida, 1710, South Africa

ARTICLE INFO

Communicated by: Bell Gavin

Keywords:
Silicon
Defect-engineering
Device fabrication
Electrical characterisation
Radiation sensors

ABSTRACT

A change in current-voltage (*I–V*) and capacitance-voltage (*C–V*) properties of silicon (Si) diodes due to the doping of the material with iron (Fe) is presented. The deviation of diode *I–V* behaviour from normal exponential to ohmic behaviour indicates that the conduction mechanism is dominated by generation-recombination (*g-r*) centres after Fe doping. The effects of *g-r* centres are more pronounced at low-frequency *C–V* measurements, where the low-mobility minority carriers are active. Due to the recombination of charge carriers, the charge ejection rate out of the space charge region (SCR) is low and less dependent on frequency measurements, possibly, showing that as they dominate the conduction mechanism, *g-r* centres are stable at one level in the band gap of Si. The results presented here are very important since they explain the properties of *g-r* centres and they show that in Si, Fe exhibits properties similar to dopants (Au and Pt) found responsible for the improvement of Si radiation-hardness.

1. Introduction

Silicon radiation detectors are devices used for scientific research in astrophysics, nuclear physics, and high-energy physics experiments [1–3]. The detectors have been preferred among others because of the material thermal stability, making the detectors operate at a temperature higher than room temperature. They are also mechanically rigid, needing no special supporting structures during operation. The large density of Si offers average energy loss per unit length, which makes the production of thin detectors a possibility without losing the ability to produce measurable signals [4]. Despite all these unique advantages, the performance of these devices gets deteriorated by the same radiation they intend to detect. This failure is attributed to defect levels created within the band gap of Si by incident radiation. The radiation-induced defect levels change electrical properties, hence, the instability of the detectors when exposed to extreme radiation conditions [5,6]. The performance, therefore, of the detectors needs to be improved for current and future use.

Studies have shown that the desired performance of the detectors can be achieved by engineering defects in Si through doping [7–9]. In these studies, defects in Si are introduced in a controllable manner such that the material properties are improved for radiation sensing applications. A controllable manner, implies the dopants, the density of the dopants, and the doping method [7,8]. As it is found to improve radiation-hardness, however, doping also increases the leakage current, limiting the radiation sensitivity of the material-based detectors. Further studies on defect-engineering are necessary to have the sensitivity of the devices not compromised at the expense of radiation-hardness of Si.

Gold (Au) and platinum (Pt) are promising dopants to improve the properties of Si for the fabrication of stable detectors during operation [7,8]. The improvement of the properties is associated with midgap defect (0.56 eV), a defect level positioned at the centre of the band gap, created by Au and Pt. This level is responsible for ohmic *I–V* diode behaviour since at this position the charge generation rate (*g*) is the same as the recombination rate (*r*). Thus, the Fermi energy of the material with a high density of midgap defects is pinned at an intrinsic position. At this position, the Fermi energy is independent of incident radiation [10]. However, Au and Pt create other defect levels that are responsible for a change in conductivity, rendering the material useless for radiation detecton applications. This shortcoming has initiated an urgent need to find other suitable dopants in a study to improve the properties of Si for radiation detection applications.

Iron (Fe) as a common element in nature that belongs to the transition metal group can be introduced into Si crystals [11]. Fe introduces deep levels into the band gap of Si generating minority carriers in *n*-Si material [12]. These minority carriers recombine with the excess

* Corresponding author.
E-mail address: moloisj@unisa.ac.za (S.J. Moloi).

https://doi.org/10.1016/j.ssc.2021.114575
Received 3 May 2021; Received in revised form 13 September 2021; Accepted 21 October 2021
Available online 23 October 2021

majority carriers, reducing the density of majority carriers in *n*-Si, hence increasing the resistivity of the material. However, Fe-induced defect level at E_C -0.55 eV was reported to be a donor level in the band gap of Si [13] where E_C is the conduction band. This donor level is expected to contribute to the density of charge carriers, reducing the resistivity of the device fabricated on Fe-doped *n*-Si. The effects of Fe-doping on the resistivity of the material are, therefore, a subject of interest. Further studies on Fe-doped *n*-Si reported two deep levels, E_V +0.40 eV and E_C -0.55 eV [14,15] in the band gap of Si, where E_V is the valence band energy. The defect level of the primary interest was that close to midgap (~0.56 eV) which was observed to be induced by Au and Pt. It is, therefore expected that in Si, Fe would exhibit similar properties as those of Pt and Au because of midgap which is common for these metals.

In this work, the *I–V* and *C–V* measurements were carried out on diodes fabricated on undoped and Fe-doped *n*-Si. Fe was implanted at the energy of 160 keV to the fluence of 10^{17} ion/cm^2. The objective of this study was to establish a change in electrical properties of the diodes due to Fe-doping and compare the obtained results with those presented in the literature based on Au- and Pt-doped Si diodes.

2. Experimental details

2.1. Material preparation

In this study, an *n*-type Si wafer (111) polished on one side was diced into 0.9 cm × 0.9 cm square pieces. The resistivity of the material was quoted by the supplier, Semiconductor wafer Inc., ranging from 1 to 20 Ω-cm with a thickness of 275±25.0 μm. The level of impurities was not provided by the supplier and the doping density was evaluated using the *C–V* technique as 7.9×10^{12} cm^{-3}. The substrates were cleaned with an ultrasonic cleaner, successively using methanol, acetone, trichloroethane, and de-ionized water to remove any dirt and handling grease. Afterward, they were dipped into 20% hydrofluoric (HF) solution to remove the oxide layer. The substrates were then blow-dried using nitrogen gas [16] before loading into a high-vacuum chamber for implantation. The pieces mounted on a holder labeled C17 were implanted with 160 keV Fe using the Varian-Extrion 200-20A2F ion implanter at iThemba LABS (Gauteng), South Africa to the fluence of 10^{17} ion/cm^2.

The implantation of Fe in Si at 160 keV was simulated using Stopping and Range of Ions in Matter (SRIM/TRIM-2013) [17]. The Fe interactions with Si atoms and modes of its energy loss were simulated to estimate the penetration depth and dopant concentration and were found to be ~134 nm and 2.6×10^{20} atom/cm^3, respectively. The electronic energy loss and nuclear energy loss were calculated to be 7.15 keV/nm and 8.38 keV/nm, respectively indicating that the nuclear part is the dominant mechanism of the energy loss per unit length in Si crystal. The information about the occupation states of Fe in Si is available in literature [18–22].

2.2. Diode fabrication

Schottky diodes were fabricated on undoped and Fe-doped crystalline *n*-Si. Before diode fabrication, Si pieces were cleaned again using the standard procedure [15]. The pieces were then loaded into an evaporation chamber for the formation of Schottky contacts. The contacts were achieved by evaporation and deposition of 250 Å gold through a mask of 0.6 mm diameter holes to form the Schottky contacts. The ohmic contact was then realized by evaporation and deposition of 200 Å aluminium onto the unpolished surface of the pieces. The deposition was done at room temperature at 10^{-6} mbar and the rate of 1 Å/s using an Edwards AUTO 306 thermal vacuum deposition system. The finished devices, each consists of 6 diodes on a piece and with one common ohmic contact. An oxide layer of 10–30 Å thick is always present on the surface even after etching Si wafers with HF solution [23]. The effects of the oxide layer on the diode properties are, therefore, assumed common to all the diodes since they were fabricated under the same conditions. Thus, a change in diode properties would be due to Fe-doping. The fabricated diodes were labeled undoped and doped diodes, referring to the one fabricated on undoped and Fe-doped *n*-Si, respectively. A schematic showing gold and aluminium as the Schottky and ohmic contacts, respectively, is shown in Fig. 1.

2.3. Device characterization

Devices in this work are Schottky diodes that were fabricated on undoped and Fe-doped *n*-Si. Studies on these diodes could lead to a celar understanding of properties of *p-n* junction diodes that are used in radiation sensing applications since they both have similar backgraoud and working principle. The diodes were characterized by *I–V* and *C–V* techniques respectively, using a Keithley 6487 picoammeter with a voltage source and an Agilent 4263B LCR meter. The *C–V* measurements were carried out at frequencies 100 Hz, 120 Hz, 1 kHz, 10 kHz, and 100 kHz offered by LCR meter. The measurements were taken with the devices placed in the dark and at room temperature. The data were taken over the range of −2 to 2 V to ensure that tunnelling electrons overcome thermionic emission [6]. At voltages above ±2 V, series resistance comes into play, and the forward current saturates with the reverse current less dependent on the applied voltage. Throughout the experiments, 1 s was maintained as the time between measurements to allow the device to stabilize. A microscope attached to the probe station was used to ascertain the contact between the fabricated diode and the probes.

3. Results and discussion

3.1. Current measurements

Fig. 2(a) shows *I–V* characteristics of the undoped diode in a logarithmic scale. The forward current has three linear regions in Fig. 2(a) with different slopes of 1.2, 5.4, and 2.7, respectively. These regions are used to study the conduction mechanism in the device, which provides the power-law performance of current, i.e., $I \propto V^m$ [24] having different values of m (slope of the linear region) for different regions. When $m \approx 1$, the dominant mechanism in the region is ohmic, indicating that current is directly proportional to the applied voltage. The ohmic behaviour is due to the domination of the thermally generated current over the injected free carrier generated current in the depletion region [24]. When $m \approx 2$, space charge limited current (SCLC) mechanism is dominant in the region, indicating that the current and voltage are related by a quadratic relationship [24]. The existence of the SCLC mechanism is observed when the traps present in SCR are partially filled or filled. Furthermore, trapped charge current limited (TCLC) occurs when $m > 2$ with V^m dependence of current [24]. TCLC is a modification of SCLC with exponentially distributed surface states dominating the

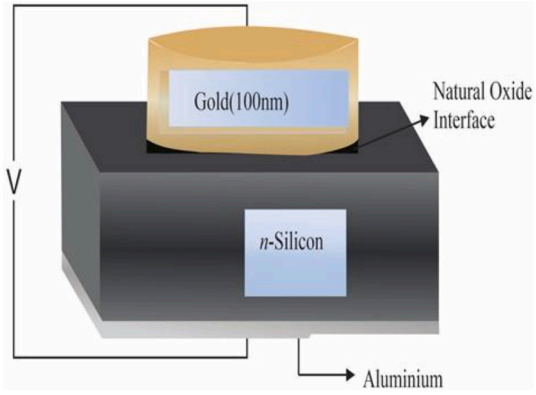

Fig. 1. Schematic diagram showing gold as Schottky contact and aluminium as ohmic contact. (For interpretation of the references to colour in this figure legend, the reader is referred to the Web version of this article.)

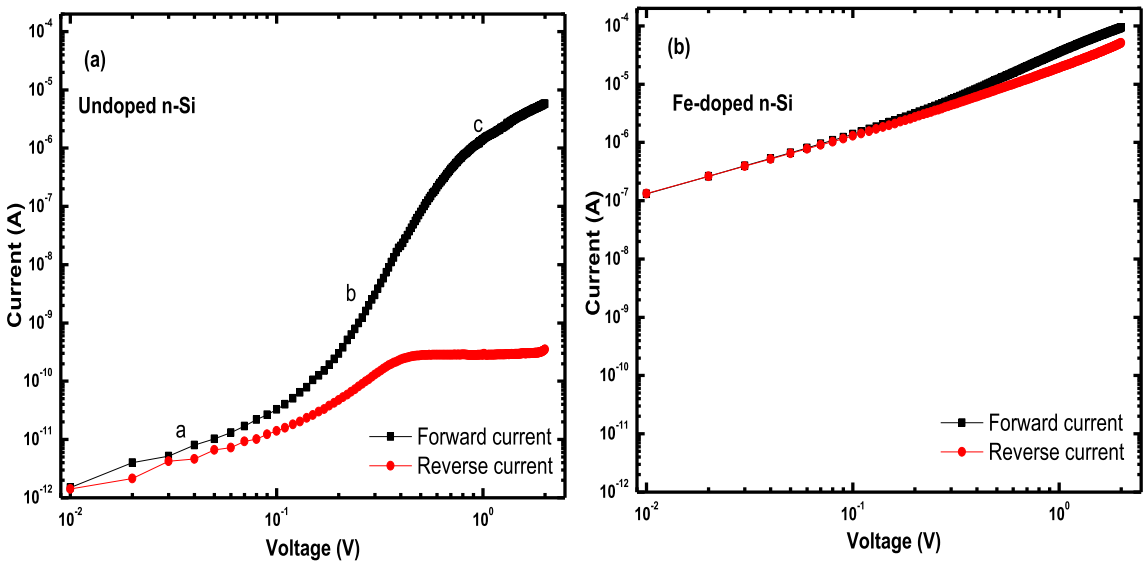

Fig. 2. Current-voltage characteristics of the diodes fabricated on undoped (a) and Fe-doped (b) n-Si in logarithmic scale.

region.

The slope of the first region is close to unity indicating that the dominant current mechanism is ohmic in this region. The second region with the slope of 5.4, indicates TCLC the dominant current mechanism for this region is SCLC with a discrete trapping level [24]. Based on the SCLC mechanism, when there is an increase in applied voltage, the injection of charge carriers from the electrode to SCR increases. The slope of the third region is 2.7, corresponding to the trap-filled limit [24,25]. As expected, for the undoped diode in Fig. 2(a) the forward current is higher than the reverse current throughout the voltage range, indicating the conduction mechanism is dominated by majority carriers.

The logarithmic *I–V* characteristics of the diode fabricated on Fe-doped *n*-Si in Fig. 2(b) show a linear region in the reverse bias trend with a slope of 1.00 indicating that the dominant current mechanism is ohmic throughout the voltage region. But two linear regions were identified on the forward current trend, with slopes, 1.09 and 1.52, respectively, close to unity, indicating that the dominant current mechanism at each region is ohmic. The observed high ohmic region confirms that Fe creates generation-recombination (*g-r)* centres in *n*-Si [26] and at the implantation fluence of 10^{17} ion/cm^2, the density of *g-r* centres is sufficient to dominate the charge distribution mechanism in the material. The ohmic behaviour occurs because *g-r* centres are positioned at 0.56 eV, in the band gap of Si and they interact with both bands such that the carrier generation rate is the same as the recombination rate [8]. Here, the densities of charge carriers injected into SCR are equal, making the material intrinsic-like [7]. Introducing Fe has resulted in an increase in the current for the whole voltage range, implying that the resistivity of the material has decreased after doping. Thus, doping with Fe results in introducing *g-r* centres, defects responsible for ohmic behaviour.

The rectification ratio, a ratio of forward current to reverse current at 2 V of an undoped diode is 1.60×10^4 while that of Fe-doped diode is 1.84. The evaluated high rectification ratio for undoped diode has been reported earlier [6,27] and it is attributed to ideal diode properties. A decrease in the rectification ratio after Fe-doping indicates that the diode rectifying behaviour has been lost. Losing rectifying behaviour is tied to the increase (decrease) in the concentration of minority (majority) carriers. In our case, both trends (reverse and forward current) have increased indicating that carrier densities have increased, with the rate of minority carrier density being higher than that of majority carriers. The results presented here indicate that the rectification ratio can be used to evaluate the deviation of diode behaviour from rectification to ohmic. A rectification ratio of unity indicates that the ohmic behaviour and the diode conduction mechanism is dominated by *g-r* defect centres. These defects are positioned at the centres of the band gap where they interact equally with both bands. The rectification ratio evaluated on Fe-doped diode is not unity and the trends are not equal at 2 V indicating that the density of *g-r* centres cannot cause the device to be ohmic for the whole voltage range.

The semilogarithmic *I–V* characteristics of the undoped and Fe-doped *n*-Si diodes are presented in Fig. 3. The trend for undoped *n*-Si diode exhibits perfect rectifying behaviour with a great difference between the reverse and forward currents. But the rectifying behaviour has been lost in the Fe-doped *n*-Si diode due to Fe-induced defects which have increased the current trends. A linear trend is observed at low voltages in both diodes but disappears at about 0.50 and 0.25 V on undoped and Fe-doped diodes respectively, giving rise to a downward curvature observed at the high voltage region in both diodes. The deviation of the trends from linearity results from the series resistance (R_s) and interface states [28]. The linear region in the forward current trend of Fe-doped *n*-Si is smaller, suggesting that Fe-induced defects affect the diode series resistance.

Based on the thermionic emission theory, the current of Schottky

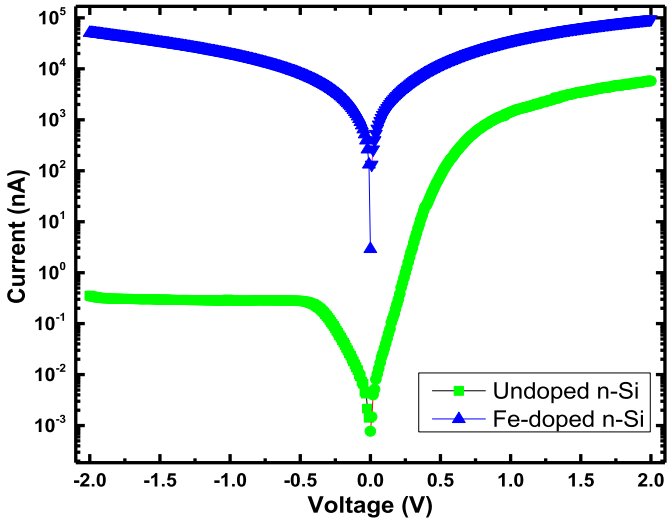

Fig. 3. Semi-logarithmic I–V characteristics of Schottky diodes fabricated on undoped and Fe-doped n-Si.

diode with R_s is given [29] as

$$I = I_s\left[\exp\left(\frac{q(V-IR_s)}{\eta kT}-1\right)\right] \quad (1)$$

and

$$I_s = AA^*T^2\exp\left(\frac{-q\varphi_b}{kT}\right) \quad (2)$$

where I_s is the saturation current, q is the electronic charge, V is the applied voltage, η is the ideality factor, k is the Boltzmann's constant, T is the temperature, A is the active diode area, A^* (= 112 A cm^{-2} K^{-2}) is the effective Richardson constant for *n*-type Si and φ_b is the Schottky barrier height. η is determined from the slope of the linear region of the forward bias ln *(I)–V* characteristics as

$$\eta = \frac{q}{kT}\frac{dV}{d\ln(I)}. \quad (3)$$

The Schottky barrier height, φ_b, on the other hand, can be calculated by substituting I_s in equation (2) as

$$\varphi_b = \frac{kT}{q}\ln\left(\frac{AA^{**}T^2}{I_s}\right). \quad (4)$$

The parameters evaluated from the linear regions of ln *(I)–V* plots were extracted and presented in Table 1. A low ln *(I)–V* linear region observed on Fe-doped *n*-Si diode makes the estimation of the parameters inaccurate, making Cheung's method a suitable alternative. In Cheung's method, the non-linear region at high voltages due to R_s is considered and is related to the forward diode current [30] as

$$\frac{dV}{d\ln(I)} = \left(\frac{\eta kT}{q}\right) + IR_s \quad (5)$$

$$H(I) = V - \left(\frac{\eta kT}{q}\right)\ln\left(\frac{I}{AA^*T^2}\right) \quad (6)$$

and $H(I)$ is given as

$$H(I) = \eta\varphi_b + IR_s. \quad (7)$$

As shown in Fig. 4, linear trends emerge from the plots of $\frac{dV}{d\ln(I)}$and *H (I) – I*, where the slopes give R_s . The values of η and φ_b are determined from the intercepts on the y-axis of $\frac{dV}{d\ln(I)}$ and *H(I) – I,* respectively. The insets in Fig. 4 are enlarged trends of $\frac{dV}{d\ln(I)}$ and *H(I) – I* for undoped *n-Si* diode.

Fig. 5 presents the junction resistance ($R_i = \partial V/\partial I$) against voltage for the fabricated diodes. A decrease in R_i at low reverse voltage in Fig. 5 (a) is due to thermal charge carriers across the SCR. As the reverse voltage increases, the SCR between the metal and Si extends into the bulk and R_i increases gently to the maximum and shows a tendency to saturate, indicating that the resistivity in Si bulk is constant. The saturation of R_i is expected since the bulk of the material is void of defects. As expected, R_i decreases as forward voltage increases due to the high density of free charge carriers through the SCR.

A decrease in R_i with negative voltage for the doped diode is observed in Fig. 5(b) which indicates there are charge carriers injected into the SCR. An absence of R_i saturation with the applied reverse voltage in Fig. 5(b) indicates that the induced defect density decreases with Fe penetration depth in the bulk. The trend for doped diode would not decrease indefinitely since at a certain voltage higher than −2 V, R_i would be ~6×10^6 kΩ and then remain independent of the voltage. This voltage would be associated with the maximum penetration depth of ~134 nm estimated using TRIM calculations presented earlier. In forward bias, R_i decreases due to the high density of free charge carriers through SCR leading to the conduction in the diode.

Table 1
The electrical parameters obtained from *I–V* characteristics of undoped and Fe-doped *n*-Si diodes.

	ln *(I)–V*			$\frac{dV}{d\ln(I)} - I$		*H (I) – I*	
Diodes	I_s (nA)	η	ϕ_B (eV)	R_s(k Ω)	η	R_s(k Ω)	ϕ_B (eV)
Undoped	0.003	1.79	0.94	20.0	1.91	231.0	0.95
Doped	580.0	5.80	0.63	2.00	1.00	20.00	0.80

The minimum value of R_i at high forward bias corresponds to R_s while the maximum value of R_i in the reverse bias corresponds to the shunt resistance (R_{sh}) [31–33]. The values of R_s and R_{sh} for undoped diode are 309 kΩ and 6 × 10^6 kΩ, respectively, while those of Fe-doped *n-Si* diode is found to be 21 kΩ and 80 kΩ, respectively. The obtained values of R_s and R_{sh} for the undoped diode are higher than those reported on Au/*n-Si* [26] and Au/Bi-doped PVA/*n-Si* type SBDs [32]. The low (high) values for R_s (R_{sh}) on the undoped diode confirm the diode's good rectifying quality. The values of R_s and R_{sh} decreased indicating that the density of free charge carriers has increased after doping Si with Fe.

The evaluated saturation current for an undoped diode was 0.003 nA, lower than the 0.018 nA obtained on Au/PLiMMA/*n*-Si [34] indicating that our diode is well fabricated. The observed increase in saturation current to 580 nA after doping further indicates that Fe-induced defects responsible for charge carriers leading to a decrease in resistivity of the material.

The evaluated ideality factor for the undoped diode obtained from ln *(I) – V* and $\frac{dV}{d\ln(I)} - I$ plots are 1.79 and 1.91, respectively. These values are close to each other with a difference of 0.12, which could be due to the existence of the interface states, series resistance, and the voltage drop across the interfacial layer [35]. A value of 1.55, was reported on Au/polyvinyl alcohol (Co, Zn-doped)/*n*-Si [36] and that of 2.31, was reported on Au/Bi-doped PVA/*n*-Si [31]. Though η evaluated in this work indicates a non-ideal diode behaviour, it falls within the range of those reported before indicating that the diodes were well fabricated.

The high value of η confirms that the current mechanism is not only due to thermionic emission but also the tunneling mechanism. The tunneling mechanism could be due to the SiO_2 layer formed between Au and Si resulting in a recombination of charge carriers through the interface states. Therefore, the total current for the undoped diode is the combination of current for the undoped *n*-Si diode due to thermionic emission and tunneling mechanism [37].

The value of η for Fe-doped diode evaluated using ln *(I)–V* method was found to be, 5.80, higher than that for undoped diode indicating that other diode conduction mechanisms than thermionic emission and tunneling mechanisms have been introduced after doping Si with Fe. The ideality factor for the Fe-doped diode evaluated using $\frac{dV}{d\ln(I)} - I$ method is 1.00, indicating a perfect diode behaviour despite the trend in Fig. 2(b) showing otherwise. The ideality factor of unity evaluated using Cheung's method probably indicates that the parameter is less dependent on defects induced in the material, hence meaningless when the diode conduction mechanism is dominated by charge carrier distribution in Si bulk.

The Schottky barrier height of the undoped diode was calculated from the y-intercept of the ln*(I)–V* and the *H(I) – I* plots. The two methods yielded similar values of 0.94 and 0.95 eV, respectively. These values are close to 0.86 and 0.84 eV, reported on Al/OG/*n*-Si device [35]. A decrease in the Schottky barrier height to 0.63 eV indicates that the energy required to have a considerable charge carrier density to contribute to the measured current has decreased after doping with Fe. This decrease in barrier height, as observed on the irradiated Si diode [38], shows that Fe-induced defect levels are responsible for an increase in carrier density through SCR. This increase in carrier density results in an increase in material conductivity, hence, a decrease in R_s as observed in Table 1.

The R_s evaluated using different methods are different. This

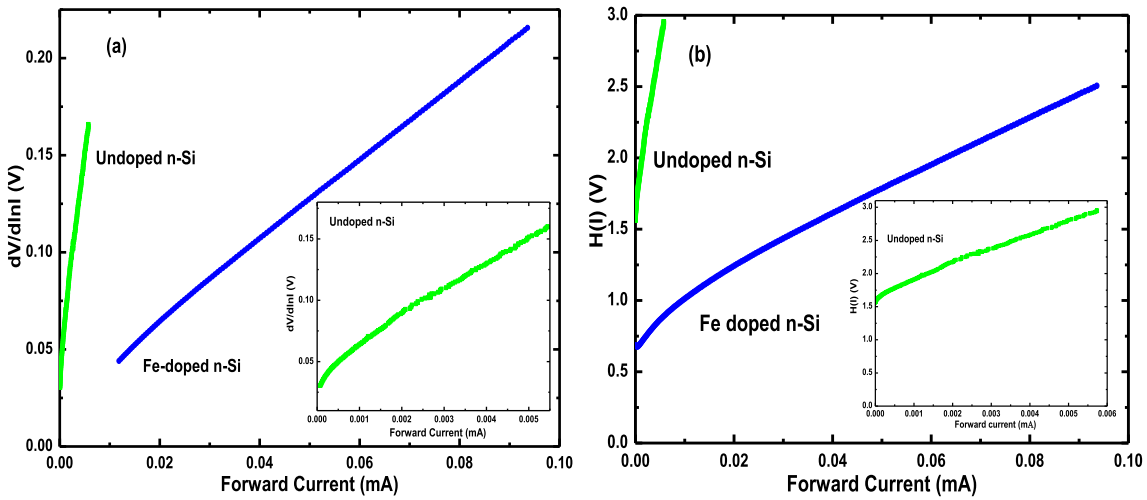

Fig. 4. $\frac{dV}{d\ln(I)}$– I (a) and H(I) – I (b) plots for diodes fabricated on undoped and Fe-doped n-Si.

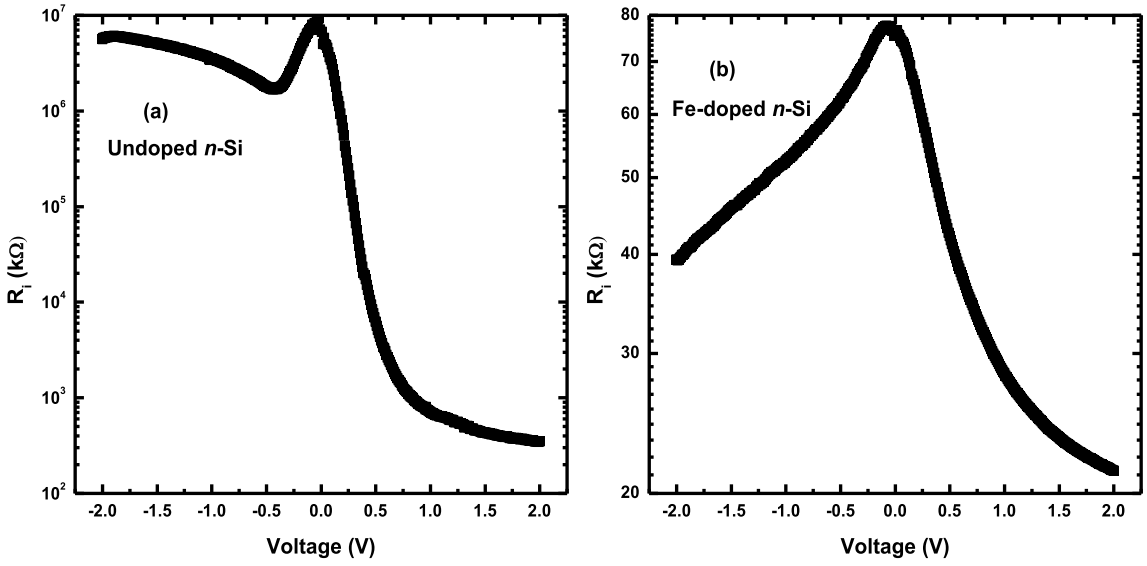

Fig. 5. *R_i – V plots of undoped (a) and Fe-doped (b) n-Si diodes.*

discrepancy in R_s was also reported in Au/Pyronin-Y/*p*-Si/Al Schottky diode and was explained in terms of an increase in the current rate due to space charge injection in an electric insulating layer at high voltage region [39]. The difference in values in Table 1, therefore, shows there is a formed insulating layer at *m-s* interface. The formed interface layer could be SiO_2 since oxygen is always present on Si surface even after chemical treatment of the wafer. Furthermore, the values of η and φ_B presented in Table 1 are also different, possibly due to the different methods used to evaluate them.

3.2. Capacitance measurements

The capacitance of the Schottky diode is defined in terms of applied reverse bias [40] as

$$C = A\sqrt{\frac{q\varepsilon_s\varepsilon_0 N_d}{2(V_{bi}+V)}} \tag{8}$$

where ε_s is the dielectric constant of the semiconductor, ε_0 is the dielectric constant of free space, N_d is the doping density, V_{bi} is the built-in voltage, and V is the applied voltage. When the diode is connected in reverse bias, the depletion region increases with applied voltage. Factors like oxide layers, interface states, and series resistance are not put into consideration in the capacitance, though in reality they exist. These factors introduce an anomalous *C–V* characteristic because any voltage applied across the diode would cause charge carriers passing through them [41].

Fig. 6 shows *C–V* characteristics of the fabricated diodes at different measurement frequencies. The capacitance is independent of the voltage at low voltage ranges, 0–0.4 V and 0–0.7 V, for undoped and Fe-doped diodes, respectively, showing that the conduction mechanism is controlled by the interface states due to the SiO_2 layer formed between Au and Si surface [42]. The capacitance decreases with an increase in measurement frequency for the same voltage to show that charge carriers at the interface follow the applied alternating current (ac) signal [42,43].

The capacitance for the undoped diode starts to decrease at voltages higher than ~0.41 V indicating that charge carriers are withdrawn from SCR. The results in Fig. 6(a), indicate that the formed SCR starts at ~0.41 V. For a diode fabricated on *p*-GaN, SCR was found to start at 0.6 V [44]. The results obtained from *C–V* measurements complement the *I–V* data and clearly explain the reverse current trend for undoped diode

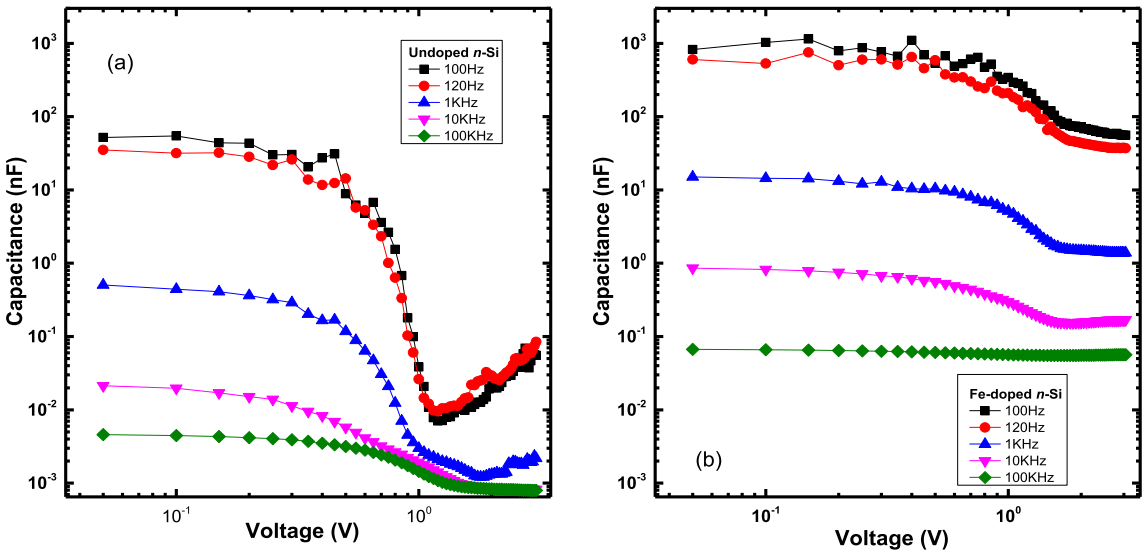

Fig. 6. *C–V characteristics at different frequencies of the diodes fabricated on un-doped (a) and Fe-doped (b) n-Si.*

presented. The *I–V* data indicated that the initial increase (decrease) of the current in Figs. 2 and 3 (of R_i in Fig. 5) is due to charge carriers generated by temperature and the *C–V* measurements confirm that the conduction mechanism at low-voltage is due to interface states because of the formed SiO_2 layer. Thus, the effects of surrounding temperature are more pronounced at low voltage, where the conduction mechanism is dominated by the interface states resulting in the ideality factor being higher than unity as presented in Table 1.

The observed drastic decrease in capacitance with voltage for undoped diode indicates that the ejection rate of charge carriers out of SCR is high. This high ejection rate could be due to the compensation of majority carriers (electrons) by minority carriers (holes) that are active at low measurement frequencies. A gentle decrease in capacitance for high measurement frequency is due to a high density of free charge carriers since low-mobility minority carriers are inactive for compensation in SCR. In Fig. 6(a) the capacitance increases after a full depletion voltage, 1.4 V, for low-frequency trends, possibly due to the ionized donors formed on the material side of SCR [45]. For high measurement frequencies at high voltage range, the capacitance is independent of voltage to show that the ionized donors do not follow the ac signal at high frequency.

The *C–V* characteristics of the Fe-doped diode, Fig. 6(b), show that a range where the capacitance is independent of voltage has increased to 0.70 V for all frequencies, indicating that the Fe-induced defects start on the surface of Si to increase the density of charge carriers. This increase in the density is confirmed by an increase in the capacitance for all measurement frequencies after doping with Fe. Because of this high density of charge carriers, the charge withdrawal rate from SCR is low. Another striking observation from Fig. 6(b) is that the capacitance for Fe-doped diode saturates at voltages higher than 1.25 V for all measurement frequencies. An increase in capacitance at high voltages for low measurement frequencies was not observed for Fe-doped diode, possibly due to charge neutralization of the ionized donors.

The results in Fig. 6(b) complement those of the *I–V* technique both showing that Fe-induced defects in Si also generate minority carriers, holes. The generation of minority carriers could then be confirmed by an increase in diode leakage current after doping. For the highest measurement frequency, 100 kHz, the injected holes do not follow the ac signal resulting in a high density of free majority carriers. A charge withdrawal rate is low, making the capacitance independent of voltage for the whole voltage range for the highest frequency measurements. Thus, a voltage higher than 3 V is needed to withdraw electrons from SCR to attain a full depletion of the device for the highest measurement frequency.

A decrease in capacitance trends at 0.41–1.25 V and 0.7–1.2 V regions for undoped and Fe-doped *n*-Si diodes, respectively, indicates the withdrawal of charge carriers out of SCR. A slope for each diode at this region, was plotted against measurement frequency in Fig. 7. The charge withdrawal rate for an undoped diode as presented in Fig. 7(a) is high since the density of minority carriers to compensate majority carriers in SCR is low and the slope decreases with frequency since the existing minority carriers become inactive as the measurement frequency increases. Because of minority carrier inactivity to compensate, the density of free carriers increases, hence a decrease in the charge withdrawal rate.

Fig. 7(b) shows that the slopes for all frequencies have decreased, indicating that the withdrawal rate has decreased after doping with Fe. A low slope for Fe-doped diode suggests that the density of holes has increased to compensate the majority carriers; hence a reduction in the free-charge carrier density in SCR after doping. The slope is less dependent on the measurement frequency, possibly showing that a charge distribution mechanism is dominated by a stable defect centre in the material. It is argued here this is a Fe-induced *g-r* centre positioned at the centre of the band gap where it generates charge carriers at the same rate as shown by ohmic *I–V* behaviour after Fe-doping. The *C–V* measurements indicate the minority carrier generation activity of these *g-r* centres are being explained by a decrease in charge withdrawal rate while the independence of the rate from measurement frequency indicates that the centres are stable.

The C^{-2} against V plots of the highest frequency measurements in Fig. 8 show the doping profile of the fabricated diodes. The plots show three and two linear regions for undoped and Fe-doped diodes, respectively, indicating a non-uniform doping density. The analysis was done for 100 kHz, a frequency where the capacitance due to interface states is minimal.

The diode parameters such as doping density (N_d), built-in voltage (V_{bi}), and barrier height (φ_b) are in Table 2 and are obtained from high linear regions of C^{-2}-V plots. $V_{bi}\left(=\frac{a}{m}\right)$ is determined from the intercept on the voltage axis of the C^{-2}-V plot as

$$\frac{1}{C^2}=2\left(\frac{V_{bi}+V}{q\varepsilon_s\varepsilon_0 A^2 N_d}\right). \tag{9}$$

where a is the intercept and m is the slope of the chosen linear region used to calculate the doping density (N_d) [46] through,

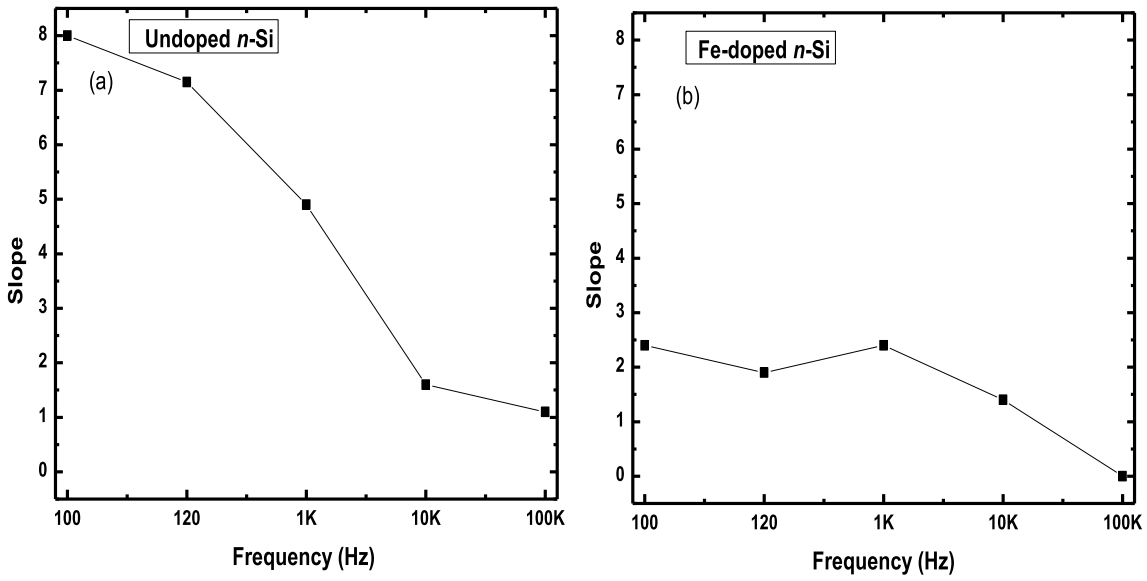

Fig. 7. *Slope as a function of the measurements frequency for (a) undoped (a) and Fe-doped (b) n-Si diodes.*

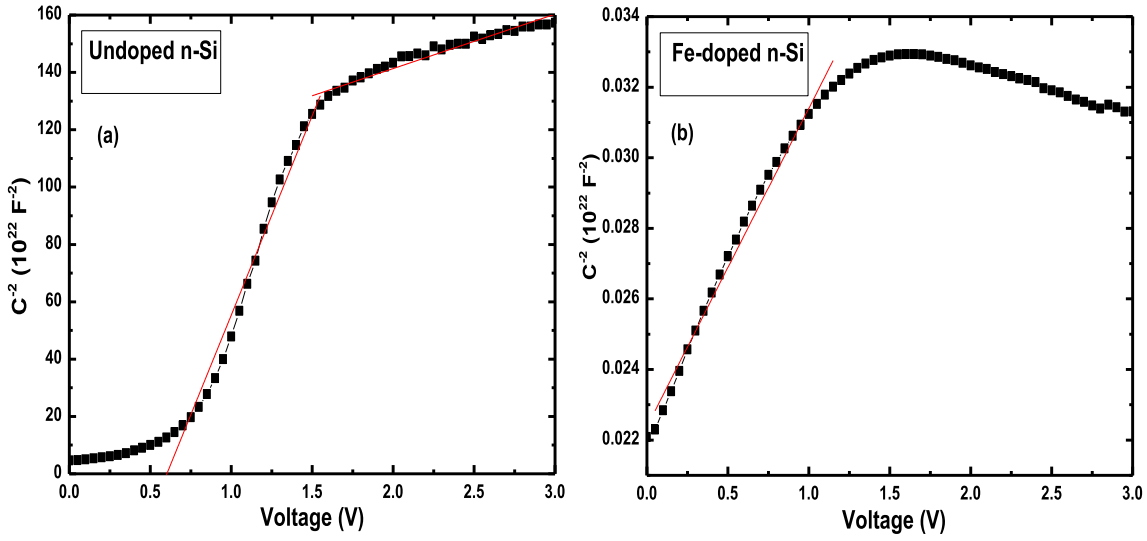

Fig. 8. *The C^{-2}–V characteristics of diodes fabricated on undoped and Fe-doped n-Si.*

Table 2
Diode parameters calculated from C^{-2} against V plots for diodes fabricated on undoped and Fe-doped n-Si diodes.

Diode	V_{bi} (V)	N_D (cm^{-3})	φ_b (eV)
Undoped n-Si	0.53	7.90×10^{12}	0.96
Fe-doped n-Si	0.24	1.96×10^{16}	0.43

$$N_d = \frac{2}{mqA^2\varepsilon_s\varepsilon_0} \quad . \tag{10}$$

The Schottky barrier height is given [47] as

$$\varphi_b = V_{bi} + \frac{kT}{q}\ln\left(\frac{N_c}{N_d}\right) \tag{11}$$

where N_c is the effective density of state in the conduction band.

The evaluated doping density of the undoped diode, 7.90×10^{12} cm^{-3}, is lower than 7.10×10^{14} cm^{-3} and 1.62×10^{15} cm^{-3} reported on Au/n-Si [46] and Sn/MB/p-Si [48], respectively, possibly due to the low concentration of doping atoms used during the production of n-Si. An increase in N_d further attests that charge carrier density has increased after doping with Fe. An increase in N_d results in a decrease in Schottky barrier height, showing that low energy is required to have considerable charge density stored in SCR. The observed negative slope of the C^{-2}-V plot at high voltages for Fe-doped diode could be an indication of conductivity-type inversion of the material from n-to p-type. This conductivity-type inversion has been reported on diodes irradiated by 1 MeV neutrons to the fluence of 1.4×10^{13} n/cm^2[49–51] and Pt-doped n-Si diode [52].

As expected, the Schottky barrier height evaluated from C^{-2}–V plot differs from the one from the I–V plot. The discrepancy for undoped and Fe-doped diodes is about 0.02 and 0.39 eV, respectively. This could be due to the inhomogeneity of barrier height and an oxide layer between the metal and the silicon surface [49]. Besides, the current in the C–V measurements is influenced by the distribution of charges at the depletion region boundary, while I–V measurement is dominated by the current that flows through the region of low Schottky barrier height [53].

4. Conclusion

In this work, Schottky diodes were well fabricated on undoped and Fe-doped *n*-Si. The diodes were characterized using *I–V* and *C–V* techniques. The diode *I–V* behaviour was found to change from normal exponential to ohmic behaviour after doping with Fe. This ohmic behaviour indicated that in Si, Fe induces *g-r* centres, defect levels positioned at the centre of the Si band gap. At this position, the induced defect levels are responsible for the generation of charge carriers at the same rate such that the charge withdrawal rate from SCR is low due to the charge compensation. *C–V* measurements show for the first time in this work that as the diode conduction mechanism is dominated by *g-r* centres, the charge withdrawal rate is independent of the measured frequency to show that the induced defect levels are relatively stable. The ohmic behaviour and high leakage current exhibited on Fe-doped diodes are similar to Au and Pt-doped diodes, indicating that Fe could be one of the suitable dopants to be used in defect-engineering studies.

Author statement

J. O. Bodunrin: student investigator, Formal analysis, Writing – original draft. S. J. Moloi: Supervision, Conceptualization, Methodology, writing-reviewing and editing,

Declaration of competing interest

The authors declare that they have no known competing financial interests or personal relationships that could have appeared to influence the work reported in this paper.

Acknowledgments

The first author acknowledges the National Research Foundation and The World Academy of Science (Grant number 116113) for student funding. This work is based on the research supported by the National Research Foundation of South Africa (Grant numbers 105292 and 114800). We would like to thank Mr. Tony Miller of iThemba LABS for Iron implantation.

References

[1] J.J. Loferski, P. Rappaport, Phys. Rev. 111 (1958) 432.
[2] S.C. Rogers, IEEE Trans. Nucl. Sci. 10 (1963) 97.
[3] G. Lutz, Semicoductor and Electronic Devices, Springer, Heidelberg, 1999.
[4] G.F. Knoll, Radiation Detection and Measurement, third ed., Wiley, New York, 2010.
[5] G. Kramberger, Nucl. Instrum. Methods Phys. Res. Sect. A Accel. Spectrom. Detect. Assoc. Equip. 924 (2019) 192.
[6] M.K. Parida, S.T. Sundari, V. Sathiamoorthy, S. Sivakumar, Nucl. Instrum. Methods Phys. Res. Sect. A Accel. Spectrom. Detect. Assoc. Equip. 905 (2018) 129.
[7] R.L. Dixon, K.E. Ekstrand, Radiat. Protect. Dosim. (1986) 527.
[8] B.K. Jones, M. McPherson, Semicond. Sci. Technol. 14 (1999) 667.
[9] G. Lindström, M. Ahmed, S. Albergo, P. Allport, D. Anderson, L. Andricek, M. M. Angarano, et al., Nucl. Instrum. Methods Phys. Res. Sect. A Accel. Spectrom. Detect. Assoc. Equip. 465 (2001) 60.
[10] V.N. Brudnyi, S.N. Grinyaev, N.G. Kolin, Phys. B Condens. Matter 348 (2004) 213.
[11] J. Wong-Leung, D.J. Eaglesham, J. Sapjeta, D.C. Jacobson, J.M. Poate, J. S. Williams, J. Appl. Phys. 83 (1998) 580.
[12] E.R. Weber, Appl. Phys. A 30 (1983) 1.
[13] K. Graff, H. Pieper, J. Electrochem. Soc. 128 (1981) 669.
[14] C.B. Collins, R.O. Carlson, Phys. Rev. 108 (1957) 1409.
[15] E. Weber, H.G. Riotte, Appl. Phys. Lett. 33 (1978) 433.
[16] B. Bera, Intl. J. Appl. Nanotechnol. 5 (2019) 8.
[17] J.F. Ziegier, J.P. Biersack, U. Littmark, The Stopping and Range of Ions in Solids, Pergamo Press, 1985.
[18] W.J. Weber, Y. Zhang, Curr. Opin. Solid State Mater. Sci. 23 (2019) 100757.
[19] J. Lefevre, J.M. Constantini, S. Esnouf, G. Pettie, J. Appl. Phys. 105 (2009), 023520.
[20] E. Hoimstrom, A. Kuronen, K. Nordlund, Phys. Rev. B 78 (2008), 045202.
[21] K. Nordlund, J. Wallenius, E. Malerba, Nucl. Instrum. Methods Phys. Res. Sect. B Beam Interact. Mater. Atoms 246 (2006) 322.
[22] K. Nordlund, S.J. Zinkle, A.E. Sand, et al., J. Nucl. Mater. 512 (2018) 450.
[23] M. Siad, A. Keffous, S. Mamma, Y. Belkacem, H. Menari, Appl. Surf. Sci. 236 (2004) 366.
[24] I. Missoum, Y.S. Ocak, M. Benhaliliba, C.E. Benouis, A. Chakera, Synth. Met. 214 (2016) 76.
[25] L.D. Rao, V.R. Reddy, AIP Conf. Proceed. 1731 (2016) 120020.
[26] M. Msinmanga, M. Mcpherson, C. Theron, Radiat. Phys. Chem. 3 (2004) 733.
[27] S. Ali, J. Bae, C.H. Lee, Electron. Mater. Lett. 12 (270) (2016).
[28] I. Dokme, Phys. B Condens. Matter 388 (2007) 10.
[29] E.H. Rhoderick, R.H. Williams, Metal-Semiconductor Contacts, second ed., Clarendon, Oxford, 1988.
[30] S.K. Cheung, N.W. Cheung, Appl. Phys. Lett. 49 (1986) 85.
[31] S. Alialy, H. Tecime, H. Uslu, Ş. Altındal, J. Nanomed Nanotechol. 4 (2013) 1000167.
[32] İ. Taşçıoğlu, U. Aydemir, Ş. Altındal, B. Kınacı, S. Özçelik, J. Appl. Phys. 109 (2011) 54502.
[33] H.S. Soliman, A.A.M. Farag, N.M. Khosifan, T.S. Solami, J. Alloys Compd. 530 (2012) 157.
[34] H. Çulcu, M. Gökçen, A. Alli, S. Alli, J. Phys. Chem. Solid. 103 (2017) 197.
[35] Ö. Güllü, Ş. Aydoğan, A. Türüt, Microelectron. Eng. 85 (2008) 1647.
[36] I. Dökme, T. Tuncay, İ. Uslu, Ş. Altındal, Synth. Met. 161 (2011) 474.
[37] P. Rosales-Quintero, A. Torres-Jacome, D. la Hidalga-Wade, C. Zúñiga-Islas, W. Calleja-Arriaga, C. Reyes-Betanzo, Superficies y vacío 21 (2008) 1.
[38] Ö. Güllü, M. Çankaya, M. Biber, A. Türüt, J. Phys. D Appl. Phys. 41 (2008) 135103.
[39] I.S. Yahia, H.Y. Zahran, F.H. Alamri, M.A. Manthrammel, S. AlFaify, A.M. Ali, Phys. B Condens. Matter 543 (2018) 46.
[40] D.K. Schroder, Semiconductor Material and Device Characterization, third ed., Wiley, New York, 2006.
[41] P. Chattopadhyay, B. Raychaudhuri, Solid State Electron. 36 (1993) 605.
[42] B. Sahin, H. Çetin, E.N. Ayyildiz, Solid State Commun. 135 (2005) 490.
[43] M.E. Aydin, F. Yakuphanoglu, J.H. Eom, D.H. Hwang, Phys. B Condens. Matter 387 (2007) 239.
[44] Z.F. Zhu, H.Q. Zhang, H.W. Liang, X.C. Peng, J.J. Zou, B. Tang, G.T. Du, Chin. Phys. Lett. 34 (2017), 097301.
[45] S.M. Sze, Physics of Semiconductor Devices, second ed., Wiley, New York, 1981.
[46] M. Msimanga, M. McPherson, Mater. Sci. Eng. B 127 (2006) 47.
[47] S.J. Moloi, M. McPherson, Radiat. Phys. Chem. 85 (2013) 73.
[48] Y.S. Ocak, M. Kulakci, T. Kılıçoğlu, R. Turan, K. Akkılıç, Synth. Met. 15 (2009) 1603.
[49] L. Agarwal, B.K. Singh, S. Tripathi, P. Chakrabarti, Thin Solid Films 612 (2016) 259.
[50] I.M. Afandiyeva, S. Demirezen, S. Altındal, J. Alloys Compd. 552 (2013) 423.
[51] D. Pitzl, N. Cartiglia, B. Hubbard, D. Hutchinson, J. Leslie, K. O'Shaughnessy, W. Rowe, et al., Nucl. Instrum. Methods Phys. Res. Sect. A Accel. Spectrom. Detect. Assoc. Equip. 311 (1992) 98.
[52] Y.K. Kwon, T. Ishikawa, H. Kuwano, J. Appl. Phys. 61 (1987) 1055.
[53] K. Tripathi, M. Sharma, J. Appl. Phys. 111 (2012), 074513.